10-nm Filaments Are Induced to Collapse in Living Cells Microinjected with Monoclonal and Polyclonal Antibodies Against Tubulin

STEPHEN H. BLOSE, DONNA I. MELTZER, and JAMES R. FERAMISCO
Cold Spring Harbor Laboratory, Cold Spring Harbor, New York 11724

ABSTRACT Cells were microinjected with four mouse monoclonal antibodies that were directed against either alpha- or beta-tubulin subunits, one monoclonal with activity against both subunits, and a guinea pig polyclonal antibody with activity directed against both subunits, to determine the effects on the distribution of cytoplasmic microtubules and 10-nm filaments. The specificities of the antibodies were confirmed by Western blots, solid phase radioimmunoassay, and Western blot analysis of alpha- and beta-tubulin peptide maps. Two monoclonals DM1A and DM3B3, an anti-alpha- and anti-beta-tubulin respectively, and the guinea pig polyclonal anti-alpha/beta-tubulin antibody (GP1T4) caused the 10-nm filaments to collapse into large lateral aggregates collecting in the cell periphery or tight juxtanuclear caps; the other monoclonal antibodies had no effect when microinjected into cells. The filament collapsing was observed to be complete at 1.5–2 h after injection. During the first 30 min after injection a few cytoplasmic microtubules near the cell periphery could be observed by fluorescence microscopy. This observation was confirmed by electron microscopy, which also demonstrated assembled microtubules in the juxtanuclear region. By 1.5 h, when most of the 10-nm filaments were collapsed, the complete cytoplasmic array of microtubules was observed. Cells injected in prophase were able to assemble a mitotic spindle, suggesting that the antibody did not block microtubule assembly. Metabolic labeling with [^{35}S]methionine of microinjected cells revealed that total protein synthesis was the same as that observed in uninjected cells. This indicated that the microinjected antibody apparently did not produce deleterious effects on cellular metabolism. These results suggest that through a direct interaction of antibodies with either alpha- or beta-tubulin subunits, 10-nm filaments were dissociated from their normal distribution. It is possible that the antibodies disrupted postulated 10-nm filament–microtubule interactions.

10-nm filament–microtubule interaction have been postulated based on studies by electron microscopy (4, 17, 26, 32, 53, 55, 58), immunofluorescence microscopy (8, 24), and biochemistry (43, 54, 55) in many eucaryotic cells. When cells are incubated in the presence of antimicrotubule drugs, such as colchicine, colcemid, or vinblastine, and cytoplasmic microtubules depolymerize (51) and the 10-nm filaments subsequently coil into juxtanuclear caps (9, 26) or collapse into large aggregates of filaments in the cytoplasm (12, 28, 33, 35). Upon release from these drugs, the microtubules rapidly reassemble into their original cytoplasmic array (51) and the 10-nm filaments then uncoil and redistribute with the majority of microtubules (26). Although it is not known if these drugs directly affect the 10-nm filaments, it is thought that as a result of microtubule depolymerization, 10-nm filaments change their distribution due to a loss of interaction with the assembled microtubules (27).

Several recent studies have shown that microinjection into living cells of antibodies against the M_r 95,000 component of vimentin-10-nm filaments (46) or antibodies directly made against the 10-nm filament protein (23, 29) cause the filaments to collapse. Although the cytoplasmic microtubules appear to remain intact it is possible that by coating the 10-nm filaments with antibody the filaments become cross-linked to themselves and/or become dissociated from their normal distribution. To further probe the possible interaction of 10-

THE JOURNAL OF CELL BIOLOGY · VOLUME 98 MARCH 1984 847-858

nm filaments with microtubules in vivo, we microinjected cells with monoclonal antibodies against either alpha- or beta-tubulin, and one polyclonal antibody against both subunits. In this paper we report that the microinjection of these antibodies causes within 1.5 h, the collapse of the 10-nm filament cytoskeleton. The consequence of microinjection did not appreciably affect protein synthesis.

MATERIALS AND METHODS

Microinjection: Gerbil fibroma cells (IMR-33, CCL-146) were grown on glass coverslips as previously described (6). Selected cells were microinjected according to the method of Feramisco (18, 19). Antibodies for microinjection were first concentrated by 40% ammonium sulfate precipitation, then dialyzed exhaustively against microinjection buffer (90 mM KCl, 10 mM Na^+/PO_4, pH 7.0), and then clarified by centrifugation at 12,500 *g* for 10 min. The antibody concentrations used for microinjection were ~10–20 mg/ml. Considering that most mammalian tissue culture cells contain ~2 mg/ml tubulin or 2–3% of the total cell protein (31, 50, 59) and that ~10% of the cell volume can be microinjected (18, 30, 60) we estimate that approximately equal amounts of antibody compared to endogenous tubulin were introduced into each cell.

Proteins: Native microtubules were purified from freshly removed brains of one day old chickens by three cycles of reversible temperature-dependent assembly as described before (7) after the method of Sloboda et al. (57). The microtubules were further subjected to ion-exchange chromatography on phosphocellulose (P-11; Whatman Laboratory Products, Inc., Clifton, NJ) to isolate 6s tubulin after Sloboda et al. (57). The alpha- and beta-tubulin subunits were separated on SDS-preparative gels containing 7.5% acrylamide-0.195% *bis*-acrylamide and isolated by electroelution of the appropriate gel bands (41). Eluted alpha- and beta-tubulin were precipitated three times with 80% acetone at 0–4°C for 0.5–1 h and then dissolved in 125 mM Tris-Cl (pH 6.8), 0.1% SDS, and 1 mM EDTA, dialysed overnight against this buffer at 4°C, and stored at −70°C.

Vimentin was isolated from the gerbil fibroma cells by high salt-nonionic detergent extraction as previously described (11). Both vimentin and cycled microtubules were used to preabsorb the antibodies in this study.

Monoclonal Antibody Production: BALB/C_{57} mice were immunized with native chick brain microtubules. The immunization schedule per mouse to produce monoclonal antibodies DM1A and DM1B was the following: day 0, 250 μg of protein emulsified in complete Freund's adjuvant (CFA)- 90% of the dose given intraperitoneally (IP) and 10% given subcutaneously (SQ); day 14, 250 μg of protein emulsified in incomplete Freund's adjuvant (ICFA) given IP and 100 μg of protein in phosphate-buffered saline (PBS) given intravenously (IV); day 25, 175 μg of protein in PBS given SQ and 175 μg of protein in PBS given IV; day 28, the spleen was removed by sterile technique and used for fusion. The immunization schedule to produce monoclonal antibodies DM3A1, DM3B3, and DM3B2 was the following: day 0, 350 μg of protein emulsified in CFA- 90% of the dose given IP and 10% of the dose given SQ; day 14, 175 μg of protein in PBS given IV and 200 μg of protein emulsified in ICFA given IP; day 28, 175 μg of protein given IV and 250 μg of protein emulsified in ICFA given IP; day 42, 500–800 μg of protein emulsified in ICFA given SQ; day 58, 1 mg of protein in PBS, slowly given IV; day 61, the spleen was removed and used for fusion. As determined by immunofluorescence staining of cultured cells, only mice with high serum titers to tubulin were selected for fusion.

Spleen cells were fused with the mouse myeloma cell line NS-1 according to the protocol of Kennett (37) as modified by Lin et al. (45) and plated into 16-mm well Linbro cloning plates. After the hybridoma cells had reached 50–75% confluency, the supernatants were tested by immunofluorescence staining of methanol fixed (−20°C, 10 min [52]) gerbil fibroma cells. A positive well was considered to give intense staining of the interphase cytoplasmic microtubules and mitotic spindles. The hybridoma cells from these positive wells were grown up in Dulbecco's modification of Eagle's medium containing 20% fetal calf serum, 100 μM hypoxanthine, and 25 μM thymidine. The cells were cloned three times in soft agar with gerbil fibroma cells used as a feeder layer after the method of Lin et al. (45). After cloning approximately 10^5 to 10^6 hybridoma cells were injected intraperitoneally into BALB/C mice that had been previously (1 wk) primed with 0.5 ml of Pristane (2,6,10,14-tetramethyl pentadecane, Aldrich Chemical Co., Milwaukee, WI). Very high titer mouse ascites fluid were then collected and used as the source of antibody.

To determine the type of heavy chain and light chain each monoclonal antibody was, hybridomas were grown in 60-mm diameter culture dishes. The supernates from confluent dishes were collected and made 40% ammonium sulfate by the addition of the solid salt. The precipitates were redissolved in a small volume of PBS and dialyzed overnight against PBS. The antibody was then placed in the center well of a double immunodiffusion plate containing 1% agarose equilibrated with PBS. The surrounding outer wells contained goat IgG (Litton Bionetics, Inc., Kensington, MD) specific for the various classes of mouse heavy and light chains Ig. Hybridoma cells were also metabolically labeled with [^{35}S]methionine (50 μCi per 16-mm diameter well) for 24 h in methionine-free media. Well supernatants were collected and subjected to *Stapholoccocus aureus* immunoprecipitation with goat-anti-mouse immunoglobulins as previously described (10). The precipitates were analysed by fluorography (13) on two-dimensional gels.

The pH of elution of the monoclonal antibodies bound to protein-A sepharose (Pharmacia Fine Chemicals, Piscataway, NJ) was determined at two pH ranges: pH 6.25 and 3.10. The monoclonal antibodies were made 0.1 M Na^+/PO_4^-, pH 8.0 and were loaded onto a protein-A sepharose column equilibrated with the same buffer. The column was washed with 4 bed vol of pH 8.0 buffer, then eluted with two successive step gradients of 0.1 M Na^+/PO_4^-, pH 6.25, and 150 mM NaCl, 100 mM acetic acid, pH 3.10. Column fractions were analysed on SDS-gels.

"Western" Immunoblots: Western immunoblots (14) were performed as described (8). After the stacking gel was removed, transfer of proteins from SDS gels to 0.45 μm Millipore nitrocellulose paper was done for 70–80 min at 90 V. The nitrocellulose paper was then incubated in 3% BSA, (bovine serum albumin, Sigma grade V) made in TBS (Tris-buffered saline: 150 mM NaCl, 50 mM Tris-Cl, 0.1% sodium azide, pH 7.5) for 12 h at 4°C. Monoclonal antibodies were diluted 1:1,000 in 3% BSA/TBS and applied to the nitrocellulose strips in a humidified chamber. After incubation for 1 h at 20°C, the strips were washed in five changes of TBS over 2 h and once in 3% BSA/TBS. ^{125}I-labeled goat IgG-anti-mouse immunoglobulins (against all heavy and light chain classes of immunoglobulins [Cappel Laboratories, Inc., Cochranville, PA]) was used at 10^6 cpm/ml in 3% BSA/TBS and applied to the nitrocellulose strips for 1 h at 20°C. The strips were then washed with five changes of TBS and dried. Autoradiograms of the nitrocellulose strips were made by exposing Kodak XAR-5 film with a Dupont Cronex Lighting-Plus AC screen for 3–12 h at −70°C. Western blots analysing polyclonal guinea pig anti-tubulin (GP1T4) were prepared as previously described (8). Proteins transferred to nitrocellulose strips were visualized by Amido black staining (8).

Solid Phase Radioimmunoassay: To each well of a 96 well polyvinyl chloride microtiter plate (Microtiter Plates cat. no. 1-220-24, Dynatech Laboratories, Inc., Alexandria, VA) 2.5 μg of alpha-tubulin, beta-tubulin, or CCL-146 vimentin was added in 50 μl of coupling buffer (50 mM Na_2CO_3, 0.1% sodium azide, pH 9.6), and coupled for 12 h at 4°C. The wells were then washed three times with 100 μl of 1 mg/ml BSA in TBS. To each well was added 50 μl of monoclonal antibody at the following dilutions: 1:200, 1:400, 1:800, 1:1,600, 1:3,200, 1:6,400, 1:12,800, and 1:25,600, and incubated for 1 h at 20°C. Following three washes with 100 μl of 0.05% Tween-80 in TBS, each well received 50 μl of ^{125}I-labeled goat anti-mouse (10^5 cpm/well) and was incubated for 1 h at 20°C. The wells were then washed three times with 0.05% Tween-80 in TBS, dried, and counted. A mouse antivimentin monoclonal SBV21 (IgG_1) was used as a control in the vimentin radioimmunoassay (RIA).

SDS PAGE and Peptide Maps: Total cell lysates were made by directly homogenizing cultured gerbil fibroma cells in SDS-sample buffer (2% SDS, 80 mM Tris-Cl, 100 mM dithiothreitol, 15% glycerol, pH 6.8) and rapidly placing the sample in a boiling water bath for 5 min. Samples were then loaded into slots of a 12% acrylamide–0.1% *bis*-acrylamide analytical SDS-gel using the Laemmli (40) buffer system and the Blattler et al. (5) gel formulation; electrophoresis in the separating gel was conducted at 250 V and gels were stained with Coomassie Blue as described (11).

Peptide maps of native chick brain 6s tubulin were generated by enzymatic cleavage with *S. aureus* V8 protease (V8) or chymotrypsin after the method of Cleveland et al. (15) modified to allow the digestion to occur under native conditions without SDS. To 134.8 μg of 6s tubulin was added 7 μg of V8 protease (Worthington Biochemcals, Freehold, NJ) in a final volume of 500 μl in buffer (50 mM PIPES-KOH, 0.5 mM $MgSO_4$, 1 mM EGTA, pH 6.9). The mixture was incubated for 30 min at 37°C and the reaction was terminated by the addition of an equal volume of 2X SDS-sample buffer and incubation in a boiling water bath for 5 min. Approximately 30 μl of sample were applied per gel slot. In a similar manner 10.5 μg of chymotrypsin (TLCK-treated, Worthington Biochemicals) was added to 134.8 μg of 6s tubulin in a final volume of 500 μl of buffer, incubated for 30 min at 37°C; and the reaction terminated as described above. About 30 μl of sample were applied per slot. Peptides were electrophoresed on SDS-gels and then transferred to Western blots as described above. Peptide maps of eluted-SDS denatured alpha- or beta-tubulin were done according to Cleveland et al. (15). To 114 μg of alpha-tubulin or 113 μg of beta-tubulin was added 1 μg of V8 protease in a final volume of 200 μl in 0.1% SDS, 125 mM Tris-Cl, 1 mM EDTA, pH 6.8. The mixture was incubated for 30 min at 37°C, then terminated as described above, and 30 μl of sample were applied per gel slot. To 114 μg of alpha-tubulin or 113 μg of beta-tubulin was added 5 μg of chymotrypsin in a final volume of 200 μl of buffer, and incubated

for 1 h at 37°C; the reaction was terminated and 30 μl of sample were applied per slot.

M_r standards used were the following: chick brain microtubule associated proteins M_r 300,000; myosin heavy chain M_r 200,000; beta-galactosidase M_r 116,500; phosphorylase-b M_r 94,000; bovine serum albumin M_r 68,000; chick brain alpha-tubulin M_r 57,000; chick brain beta-tubulin M_r 54,000; actin M_r 45,000; ovalbumin M_r 43,000; carbonic anhydrase M_r 30,000; soybean trypsin inhibitor M_r 21,000; and lysozyme M_r 14,300 as previously described (8).

[^{35}S]Methionine Microlabeling of Microinjected Cells and Two-Dimensional Gel Electrophoresis: For microlabeling, after the method of Cleveland et al. (16), a 250 μCi aliquot of [^{35}S]methionine (>600 Ci/mmol, Amersham cat. no. SJ235; dissolved in water containing 0.1% 2-mercaptoethanol) was placed in a sterile 1.8 ml NUNC vial, frozen in liquid nitrogen, and lyophilized. The label was then dissolved in 25 μl of culture media lacking methionine and used immediately for microlabeling of cells.

Glass chips of <1 mm^2 were prepared by breaking sterile glass coverslips with forceps. Cells were then seeded onto these coverslips at a low density so that between 20–30 cells attached per glass chip. The chips were then kept in 35-mm culture dishes and 24–48 h postplating all the cells on selected chips were microinjected with antibodies. The chips were then placed in the incubator for 1.5–2 h. The chips were then removed from the dish with sterile jewelers forceps and rinsed twice, 30 s each, in 37°C tissue culture media lacking methionine. The chip was then placed into a 10-μl drop of labeling media (-methionine) containing 100 μCi [^{35}S]methionine. The drop was on a small square of Parafilm in a 35-mm culture dish. After labeling for an additional 2 h in the tissue culture incubator, the chip was rinsed twice in warm media containing unlabeled methionine. At each step during the labeling the cells on the chip were checked by phase-contrast microscopy to determine that they were not damaged.

The chip was then directly placed into 20 μl of hot (100°C) SDS-sample buffer in a 1.5 ml Eppendorf tube and scrapped with an Eppendorf plastic micropipette. The sample (plus the glass chip) was rapidly placed on a boiling water bath for 5 min, the chip was then removed, the sample frozen in liquid nitrogen, and lyophilized. The sample was then dissolved into 50 μl of two-dimensional sample buffer (9.95 M urea, 4% Nonidet P-40, 2% ampholines pH 5–7, 100 mM dithiothreitol, and 0.3% SDS) at 37°C for 30 min. Acrylamide isoelectric focusing gels were cast with pH 5–7 ampholines and the second dimension was electrophoresed on 10% acrylamide SDS-gels after Garrels (22). Gel fluorography was performed as modified for [^{35}S]methionine-labeled proteins (22). Two-dimensional gels were loaded with ~120,000 cpm of trichloroacetic acid precipitable counts. The fluorograms were exposed for 1 month at −70°C. Two-dimensional gels of the monoclonal heavy and light chains were analysed with pH 3–10 ampholines and 12% acrylamide-SDS gels.

Indirect Immunofluorescence and Polyclonal Antibodies: Cells were fixed and stained for indirect immunofluorescence as previously described (6). For double label indirect immunofluorescence, comparing the distribution of two different antibodies in contrasting fluorochromes-fluorescein isothiocynate (FITC) and tetramethyl rhodamine isothiocynate (TMRITC), rabbit IgG-anti-vimentin (#240) in TMRITC and guinea pig IgG-anti-tubulin (GP1T4) in TMRITC were used as described (7) and the specificity of these antibodies has been described elsewhere (8). To analyse the distribution of mouse monoclonal antibodies, we used FITC-goat anti-mouse (Cappel Laboratories, Inc., Cochranville, PA) at ~0.7 mg/ml. To reduce the observation of FITC-stimulated TMRITC fluorescence, we included the Zeiss barrier filter BP 520–560 (cat. no. 46-79-94-9903) in the epifluorescence nose piece module.

Electron Microscopy: Microinjected cells were circled with an ink ring on the outside bottom of the culture dish using an inverted phase-contrast microscope. At selected times after microinjection the cells were fixed and processed for electron microscopy after Blose and Chacko (9). Serial en face sections of the cells were prepared (80–100 nm thick) and examined in a Philips 201 electron microscope.

RESULTS

Antibody Characterization

By double immunodiffusion analysis the monoclonal mouse immunoglobulin class was determined: DM1A, DM1B, DM3A1, and DM3B3 were IgG_1 with kappa-light chains; and DM3B2 was an IgM. DM1A and DM3A1 eluted from protein-A sepharose at pH 6.25, and DM1B and DM3B3 eluted at pH 3.10 (Table I). DM3B2, an IgM, did not bind to protein-A Sepharose. The metabolically labeled [^{35}S]methionine monoclonals were immunoprecipitated with goat anti-mouse/*S. aureus* to examine that each clone secreted only one antibody. As observed by two-dimensional gels (Fig. 1) each clone gave rise to a unique set of light and heavy chains.

To verify the specificities of the monoclonal antitubulins, we performed several analyses: the antibodies were analysed on Western blots of tubulin subunits, total cell lysates, V8, and chymotryptic peptide peptide maps of SDS-denatured alpha-tubulin, and beta-tubulin, and peptide maps of native 6s tubulin, and by binding to alpha-tubulin, beta-tubulin, and vimentin in a solid phase RIA.

DM1A and DM3A1 were anti-alpha-tubulins as determined by Western blots of tubulin subunits and total cell lysates (Fig. 2). Both bound to the same set of V8 peptides of SDS-denatured alpha-tubulin (an example of this type of experiment for the analysis of DM1A binding to V8 and chymotryptic fragments of alpha- and beta-tubulin is shown

TABLE I

Characteristics of Microinjected Antitubulin Antibodies

	Ig-class	Prot-A Sepharose elution pH	Tubulin subunit specificity	Microinjection: effect on 10 nm-filaments
Monoclonal antibody				
DM1A	IgG_1	6.25	α	+
DM3A1	IgG_1	6.25	α	—
DM1B	IgG_1	3.10	β	—
DM3B3	IgG_1	3.10	β	+
DM3B2	IgM	ND	α and β	—
Polyclonal antibody				
GP1T4	IgGs	ND	α and β	+

ND, not determined.

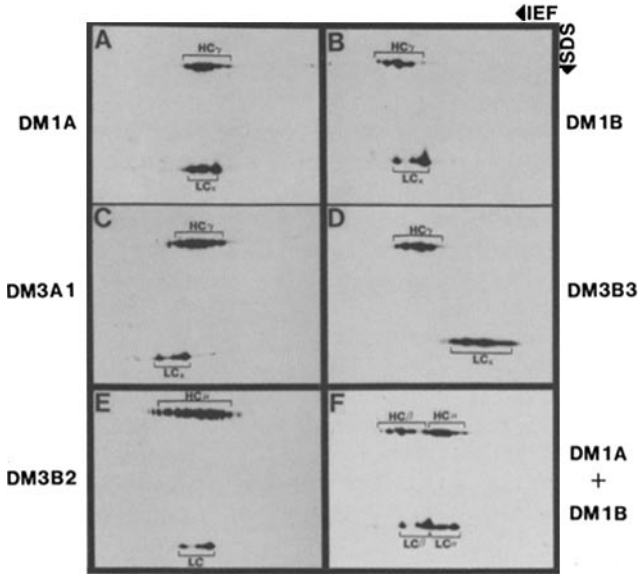

FIGURE 1 Fluorogram of two-dimensional gels of *S. aureus* immunoprecipitates of the monoclonal antitubulins metabolically labeled with [^{35}S]methionine. Each monoclonal produced a heavy chain (*HC*) and light chain (*LC*) with unique isoelectric points. The immunoglobulin class was determined by double immunodiffusion analysis: (*A*) DM1A, (*B*) DM1B, (*C*) DM3A1, and (*D*) DM3B3 were IgG_1 with HC_γ (M_r ~53,000) and LC_κ (M_r ~25,000). (*E*) DM3B2 was an IgM with HC_μ (M_r ~72,000). (*F*) DM1A (α) and DM1B (β) were mixed to show the distinct electrophoretic mobilities of the *HC* and *LC*. Isoelectric focusing gels contained pH 3–10 ampholines.

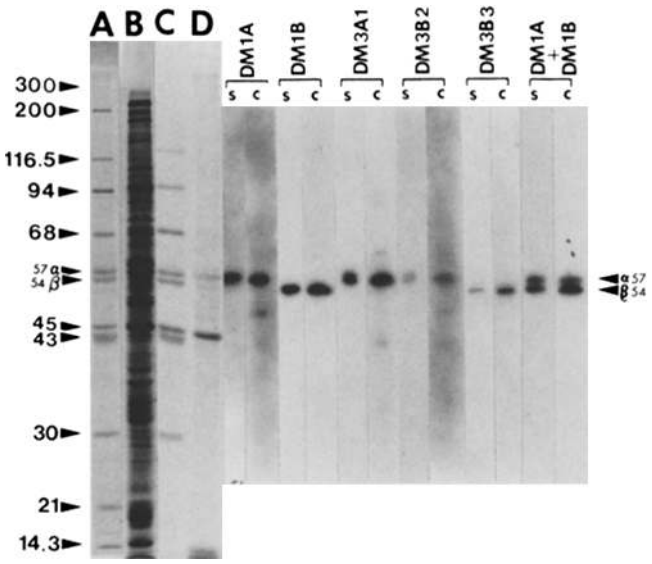

FIGURE 2 Western blot analysis of the monoclonal antitubulin binding to a total cell lysate of the CCL-146 cells and standard proteins containing brain alpha- and beta-tubulin. (Lane *A*). The M_r standards × 10^{-3}; 57_α and 54_β corresponding to alpha- and beta-tubulin, respectively. (Lane *B*) The total cell lysate. Both of these lanes were 12% SDS gels stained with Coomassie Blue. (Lanes *C* and *D*) The blots of *A* and *B*, respectively, stained with Amido black. Monoclonal antibody blots of these lanes (*s*, M_r standards corresponding to lane *A*; and *c*, cell lysate corresponding to lane *B*) revealed that DM1A and DM3A1 stained alpha-tubulin; DM1B and DM3B3 stained beta-tubulin; DM3B2 stained predominantly alpha-tubulin. The last two lanes (*DM1A+DM1B*) show that the mixing of DM1A with DM1B stained both tubulin subunits.

in Fig. 3) and the same set of V8 or chymotryptic peptides generated from native 6s tubulin (Fig. 3). DM3A1 recognized the same set of chymotryptic peptides of SDS-denatured alpha-tubulin as DM1A plus a unique peptide at M_r ~20,000 (Fig. 3). The specificity of DM1A and DM3A1 were further confirmed as anti-alpha-tubulins by solid phase RIA (Fig. 4).

DM1B had strong binding predominantly to beta-tubulin on Western blots (Fig. 2), although it weakly recognized an alpha-tubulin V8 peptide derived from native 6s tubulin (Fig. 3). This peptide was recognized by the other anti-alpha-tubulins—DM1A and DM3A1 (Fig. 3). On chymotryptic peptide maps of native 6s tubulin, DM1B recognized a single peptide that was also recognized by DM3B3, an anti-beta tubulin (see results below). DM1B recognized chymotryptic fragments of SDS-denatured beta-tubulin only (Fig. 3). The peptides of beta-tubulin generated by V8 protease were not recognized by DM1B. By solid phase RIA, DM1B bound 14 times more counts to beta-tubulin that to alpha-tubulin (Fig. 4). A similar result has been described for a monoclonal anti-beta-tubulin (TUB 2.5) with secondary activity against alpha-tubulin by Gozes and Barnstable (29).

DM3B3 was an anti-beta-tubulin as determined by Western blots of tubulin subunits and total cell lysates (Fig. 2). It did not bind to V8 peptides of native 6s tubulin, but bound to the same chymotryptic peptides detected by DM1B (Fig. 3). DM3B3 detected the same chymotryptic peptides of SDS-denatured beta-tubulin as recognized by DM1B (Fig. 3). As with DM1B, DM3B3 did not recognize any of the V8 peptides (Fig. 3). This possibly indicates that the V8 protease destroys the antigenic site. On solid phase RIA, DM3B3 reacted strongly with beta-tubulin (Fig. 5); activity against alpha-tubulin was not detected.

DM3B2, an IgM, on Western blots recognized predominantly alpha-tubulin brain subunits and alpha-tubulin of CCL-146 cell lysates (Fig. 2). On peptide maps of native 6s tubulin, DM3B2 detected peptides recognized by both the monoclonals against alpha- and beta-tubulin (Fig. 3). When DM3B2 was analysed on V8 and chymotryptic maps of SDS-denatured alpha- or beta-tubulin, it recognized the same peptides of alpha-tubulin as detected by DM1A and DM3A1, and it recognized peptides of beta-tubulin that were different from those detected by DM1B and DM3B3 (Fig. 3). On solid phase RIA, DM3B2 bound 3.5 times more counts to alpha-tubulin than to beta-tubulin (Fig. 4). Therefore, DM3B2 has activity against both alpha- and beta-tubulin subunits.

All of the monoclonals against tubulin did not detect vimentin on Western blots or on solid phase RIA (Fig. 4). The guinea pig polyclonal antitubulin (GP1T4) had both anti-alpha- and anti-beta-tubulin binding (8) (also see Fig. 8*D*).

Microinjection

Interphase gerbil fibroma cells arrange their 10-nm filaments and microtubules in similar coincident cytoplasmic arrays that span radially from the nucleus to the cell's border (Fig. 5). When these cells were microinjected with monoclonal DM1A or DM3B3 (Figs. 6 and 7), or with the polyclonal GP1T4 (Fig. 8), within 2–3 h in ~50% of cells the 10-nm filaments had collapsed into tight lateral aggregates observed in the cell periphery or cell processes (Fig. 6, *A–F*). In the other 50% of the cells the 10-nm filaments had withdrawn into tight juxtanuclear caps (Fig. 7, *A–F*). Within the first 30 min after injection only a few prominent microtubules could be observed near the cell nucleus because the injected antibody obscured the visualization, however microtubules near the cell periphery could be observed (Fig. 9). After ~1.5 h, the complete cytoplasmic array of microtubules could be observed in the same cells containing the cap of 10-nm filaments in a juxtanuclear position (Fig. 9). 3 h postinjection the 10-nm filaments remained collapsed and the microtubules maintained their usual cytoplasmic distribution (Figs. 6–9). Since it was difficult to assess microtubule distribution in the first 30 min after microinjection by fluorescence microscopy, microinjected cells were examined by serial section in the electron microscope. In all cases, microinjected cells showed assembled microtubules near the nucleus as well as the cell periphery (Fig. 10). This microtubule distribution was the same as that observed in control-injected or control-uninjected cells. As observed in Figs. 6, *B* and *E*, and 7, *C* and *E*, the distribution of the collapsed or capped 10-nm filaments could be delineated when the cells were viewed for the distribution of microtubules with FITC. These filaments were, however, red in color and could be observed because the overlap of the FITC emission (62) with the excitation wavelength of the TMRITC-antivimentin. The red fluorescence was strong enough to penetrate through the barrier filter ("bleed-through") because the vimentin staining of the collapsed 10-nm filaments was intense.

If these antibodies were first preabsorbed with assembled microtubules and then injected, the 10-nm filament collapsing was abolished, while preabsorption with CCL-146 vimentin had no effect on collapsing (Fig. 11). The microinjection of DM1B, DM3A1, or DM3B2 under identical conditions ap-

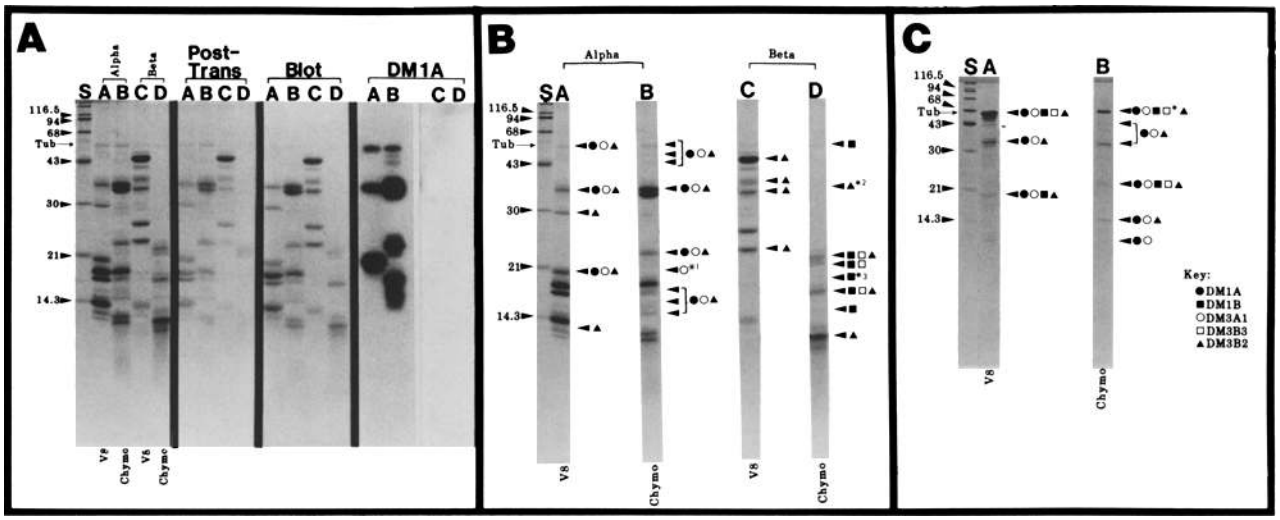

FIGURE 3 (*A*) Western blot analysis of monoclonal DM1A binding to V8 peptides (V8) and chymotryptic peptides (*Chymo*) of SDS-denatured chick brain alpha-tubulin and beta-tubulin as an example of how all the monoclonal antibodies were analysed. Peptides were prepared as described in Materials and Methods and chromatographed on a 15% acrylamide SDS-gel. Lane *S* contains the M_r standards × 10^{-3}; *Tub*, indicates the position of the tubulin subunits. Lane *A* contains the V8 peptides generated from α-tubulin; lane *B* contains the chymotryptic peptides generated form alpha-tubulin. Lane *C* contains the V8 peptides of beta-tubulin and lane *D* contains the chymotryptic peptides of beta-tubulin. These lanes are stained with Coomassie Blue. After transfer of the peptides a similar gel was stained with Coomassie Blue (*Post-Trans*) to observe the remaining peptides. Most of the peptides were transferred. The nitrocellulose blot (*Blot*) of the gel stained with Amido black showed the major peptides had transferred. *DM1A* stained a few of the alpha-tubulin peptides generated by V8 protease and chymotrypsin; it did not detect any beta-tubulin peptides. All of the monoclonal antibodies were analysed in a similar fashion on peptides generated from denatured subunits and from native 6s tubulin. All antibodies used for the Western blots were diluted 1:1,000. (*B*) Summary of antibody binding to proteolytic fragments of SDS-denatured chick brain alpha- and beta-tubulin. Lane *S* contain the M_r standards × 10^{-3}; *Tub*, indicates the position of alpha- and beta-tubulin subunits. Lane *A* contains the V8 proteolytic fragments (*V8*) of alpha-tubulin and lane *B* contains the proteoltyic fragments of alpha-tubulin digested with chymotrypsin (*Chymo*). Lane *C* contains the V8 proteolytic fragments (*V8*) of beta-tubulin and lane *D* contains the chymotryptic fragments (*Chymo*) of beta-tubulin. **1* indicates the position of an alpha-tubulin chymotryptic peptide bound by DM3A1, **2* a beta-tubulin chymotryptic peptide bound by DM3B2, and **3* a beta-tubulin chymotryptic fragment bound by DM1B that were all detected on Western blots, but were not visualized in the Coomassie-Blue-stained gels. (*C*) Summary of antibody binding to proteolytic fragments of chick brain native 6s tubulin. Lane *S* contains the M_r standards × 10^{-3}; *Tub*, indicates the position of the native 6s tubulin molecule. Lane *A* contains the V8 protease fragments (*V8*) generated from 6s tubulin. Lane *B* contains the chymotryptic peptides (*Chymo*) generated from 6s tubulin. The arrowheads on lanes *A* and *B* indicate the positions of the major peptides to which the antibodies bind. The asterisk (*) indicates some diminished binding of DM3B3 to the parent molecule relative to DM1B. The symbols in the *Key* are used to identify the respective antibody binding to the peptide fragments. The SDS-gels were 15% acrylamide.

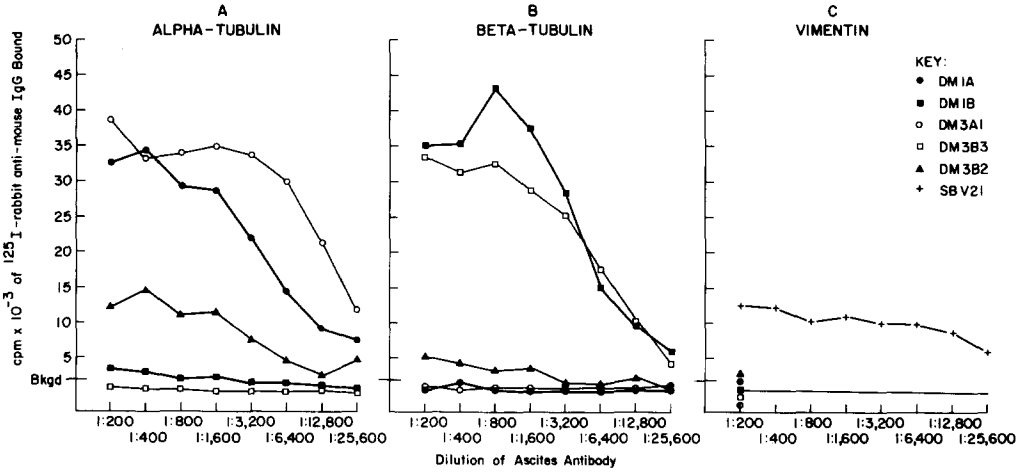

FIGURE 4 (*A*) Solid-phase RIA analysis of monoclonal antitubulins binding to chick brain α-tubulin. DM1A and DM3A1 bound the largest number of counts to alpha-tubulin, followed by DM3B2. DM1B bound a small number of counts above background to alpha-tubulin. DM3B3 binding was not detected. (*B*) Solid phase RIA analysis of monoclonal antitubulins binding to chick brain beta-tubulin. Both DM1B and DM3B3 bound large numbers of counts to beta-tubulin, with lower binding of DM3B2. DM1A and DM3A1 binding were not detected. (*C*) Solid-phase RIA of monoclonal antitubulins binding to vimentin from CCL-146 cells. No binding to vimentin could be detected for the monoclonal antitubulins. SBV21, a mouse monoclonal (IgG_1) to vimentin, was included as a control. The symbols in the *Key* refer to the respective monoclonal antitubulins. *Bkgd*, indicates background counts.

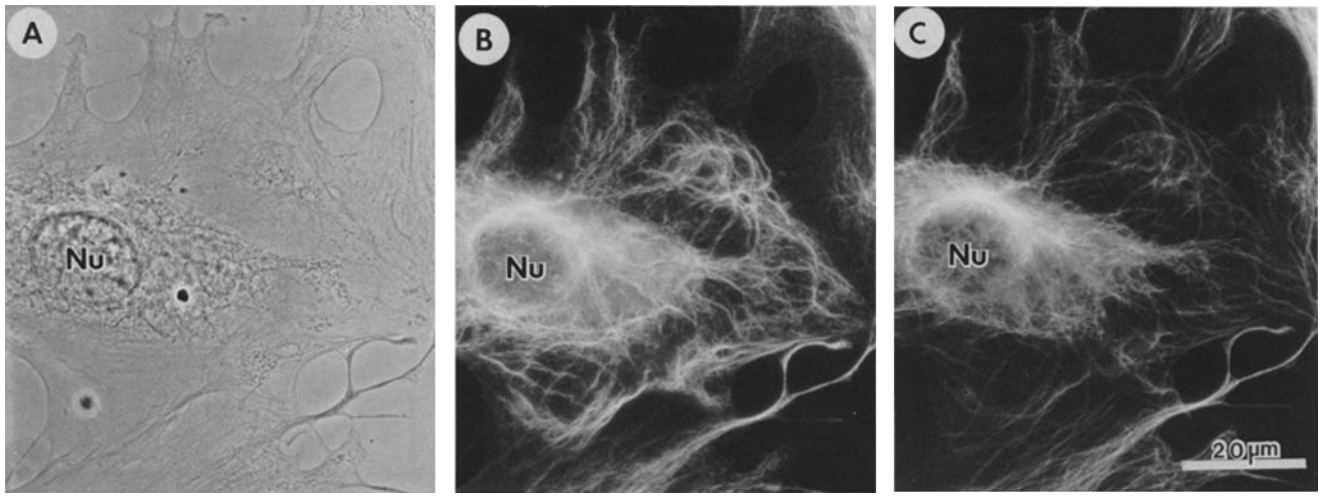

FIGURE 5 Phase-contrast (*A*) and fluorescent micrographs (*B* and *C*) of a control (uninjected) CCL-146 cell indirectly stained for vimentin with #240 antibody labeled with TMRITC (*B*) and for tubulin with DM3B3, monoclonal anti-β-tubulin, labeled with FITC (*C*). The distribution of vimentin filaments and microtubules is nearly coincident. *Nu*, nucleus. × 800.

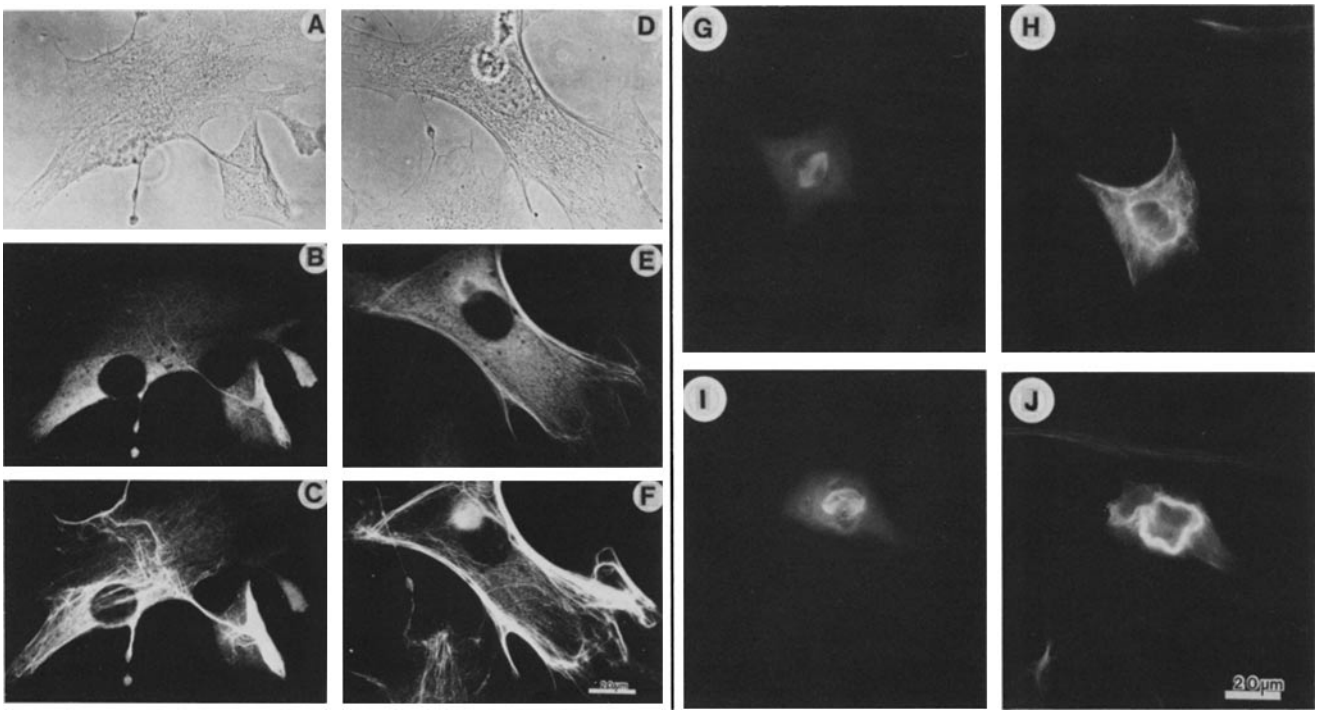

FIGURE 6 (*A–F*) Fluorescence micrographs of cells microinjected with DM3B3, monoclonal anti-beta-tubulin, and stained to observe the vimentin filament distribution at ~3 h after injection. Each triplet, (*A–C* and *D–F*, represents the same cell stained for the distribution of DM3B3 with FITC goat anti-mouse (*B* and *E*) and for the vimentin filaments with TMRITC labeled antivimentin-#240 (C and *F*). These cells represent the typical distribution of the vimentin filaments (collapsed) after being injected with monoclonal antitubulins that cause filament aggregation. The vimentin filaments were observed to collapse and aggregate in cell processes (*C*) or along the lateral margins of the cell periphery (*F*). *B* and *E* show the diffuse distribution of the microinjected antibody within the cytoplasm, however the outline of the collapsed 10-nm filaments (red in color) were observed due to FITC-stimulated TMRITC-fluorescence (see Results). (*G–J*) fluorescence micrographs of two metaphase cells 30 min after microinjection with DM3B3. Each pair, *G–H* and *I–J*, represents the same cell stained for the distribution of DM3B3 with FITC goat anti-mouse (*G* and *I*) and for vimentin filaments with TMRITC labeled #240 antivimentin (*H* and *J*). DM3B3 was visualized on the metaphase spindle microtubules (*G* and *I*); the antibody did not block assembly of the spindle to this stage. The distribution of vimentin filaments formed a cage around the spindle (28) and was not affected by the injected antitubulin. (*A–F*) × 300. (*G–J*) × 350.

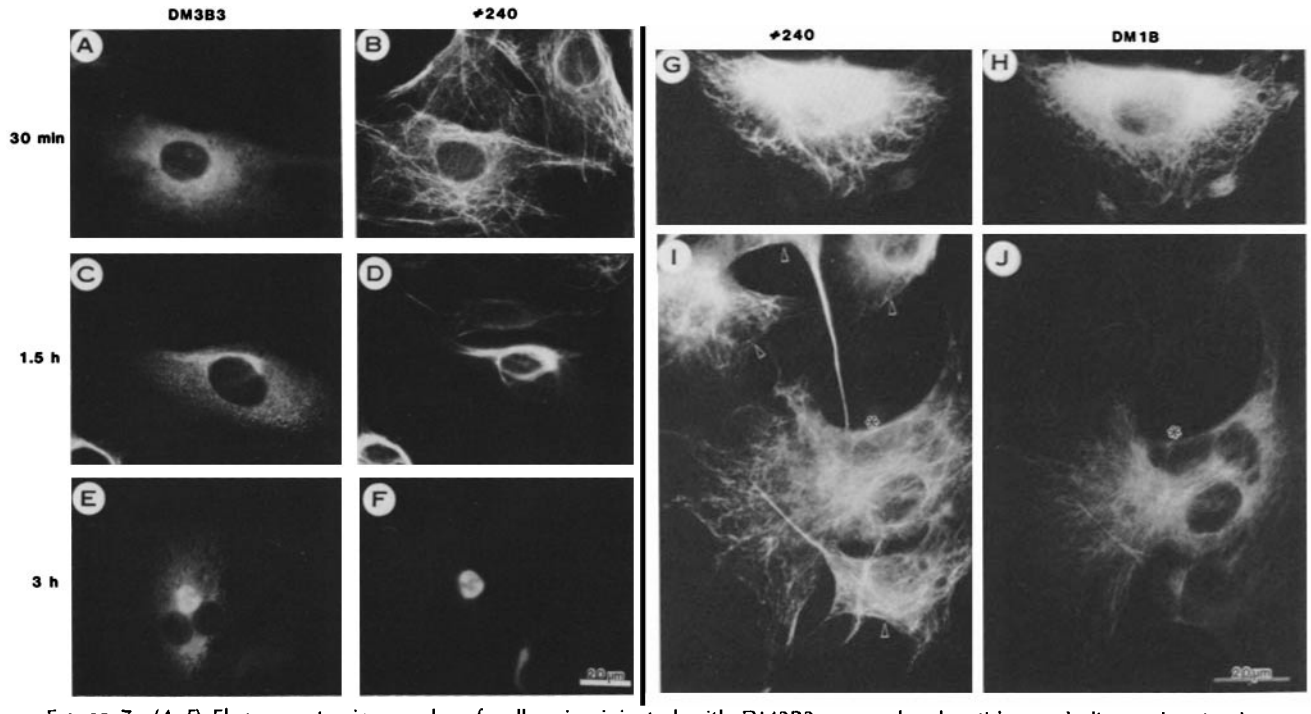

FIGURE 7 (*A–F*) Fluorescent micrographs of cells microinjected with DM3B3, monoclonal anti-beta-tubulin, and stained to observe the vimentin filament distribution at 30 min (*A* and *B*), 1.5 h (*C* and *D*), and 3 h (*E* and *F*) after injection. Each pair, *A* and *B*, *C* and *D*, and *E* and *F* represents the same cell stained for the distribution of DM3B3 with FITC-labeled goat anti-mouse (*A*, *C*, and *E*) and for the distribution of the vimentin filaments with TMRITC-labeled anivimentin-#240 (*B*, *D*, and *F*). At each time point the injected DM3B3 (*A*, *C*, and *E*) was found to be diffusely distributed in the cytoplasm. Within the first 30 min after injection the vimentin filaments (*B*) appeared to have the same distribution as the uninjected cell (see Fig. 4 *B*). By 1.5 h after injection (*D*) the vimentin filaments had collapsed next to the nucleus. At 3 h after injection (*F*) the vimentin filaments had completely moved into a tight cap next to the nucleus. In *C* and *E* the outline of the 10-nm filament caps (red in color) were observed due to the FITC-stimulated TMRITC-fluorescence (see Results). (*G–J*) Fluorescence micrographs of cells microinjected with DM1B, monoclonal anti-beta-tubulin, and stained to observe the vimentin filament distribution ~3 h after injection. Each pair, G and H and I and J, represents the same cell stained for the distribution of vimentin filaments with TMRITC-labeled antivimentin-#240 (*G* and *I*) and for the distribution of DM1B with FITC-labeled goat anti-mouse (*H* and *J*). In the injected cells (*) DM1B appeared to have no effect on the vimentin filament distribution (*G* and *I*) as compared to uninjected cells (arrowheads). The monoclonal antibody could be seen on peripheral microtubules but a diffuse fluorescence was observed near the nucleus (*H* and *J*). This was a representative example of the microinjected monoclonal antibodies that produced no apparent effect on the vimentin filament distribution (i.e., DM3A1, DM3B2, and DM1B). (*A–F*) × 325. (*G–J*) × 500.

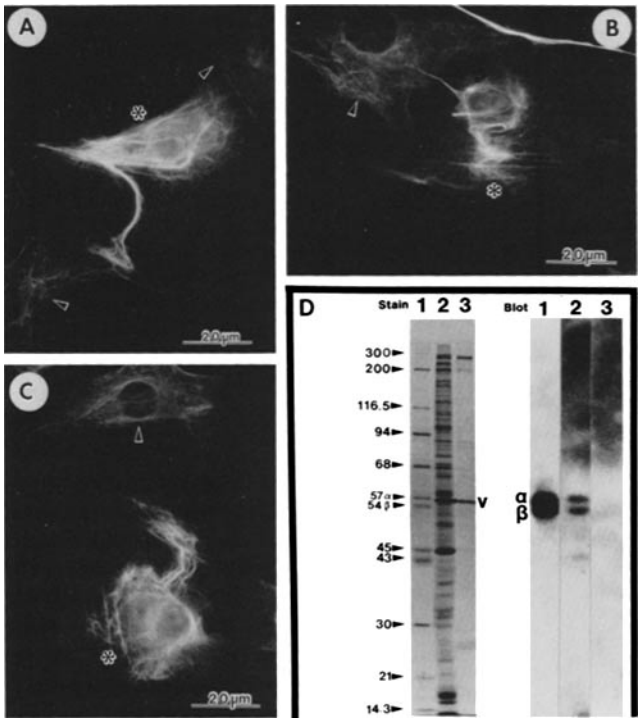

FIGURE 8 Fluorescence micrographs of CCL-146 cells microinjected with polyclonal guinea pig antitubulin (GP1T4) and stained to observe the vimentin filament distribution (*A*, *B*, and *C*) 3 h postmicroinjection. In each case (*A*, *B*, and C) the filaments were induced to collapse into aggregates in the injected cell (*) as compared to uninjected cells (arrowheads). Western blot analysis of the polyclonal antitubulin, GP1T4 (D). Lane *1*, are the M_r standards × 10^{-3}, including chick brain alpha-(57_α) and beta-(54_β) tubulin; lane *2*, represents the total CCL-146 cell lysate with the position of vimentin indicated by the dark circle; and lane *3*, partly purified CCL-146 vimentin (*v*) isolated by high salt-non ionic detergent extraction (11). These lanes are stained with Coomassie Blue (*Stain*) and correspond to the same lanes on the Western blot (*Blot*). The polyclonal antitubulin stained both the alpha and beta subunits from chick brain (*Blot*, lane *1*) and CCL-146 cells (*Blot*, lane *2*); the antibody had no reaction with CCL-146 vimentin (*Blot*, lane *3*). (*A–B*) × 450.

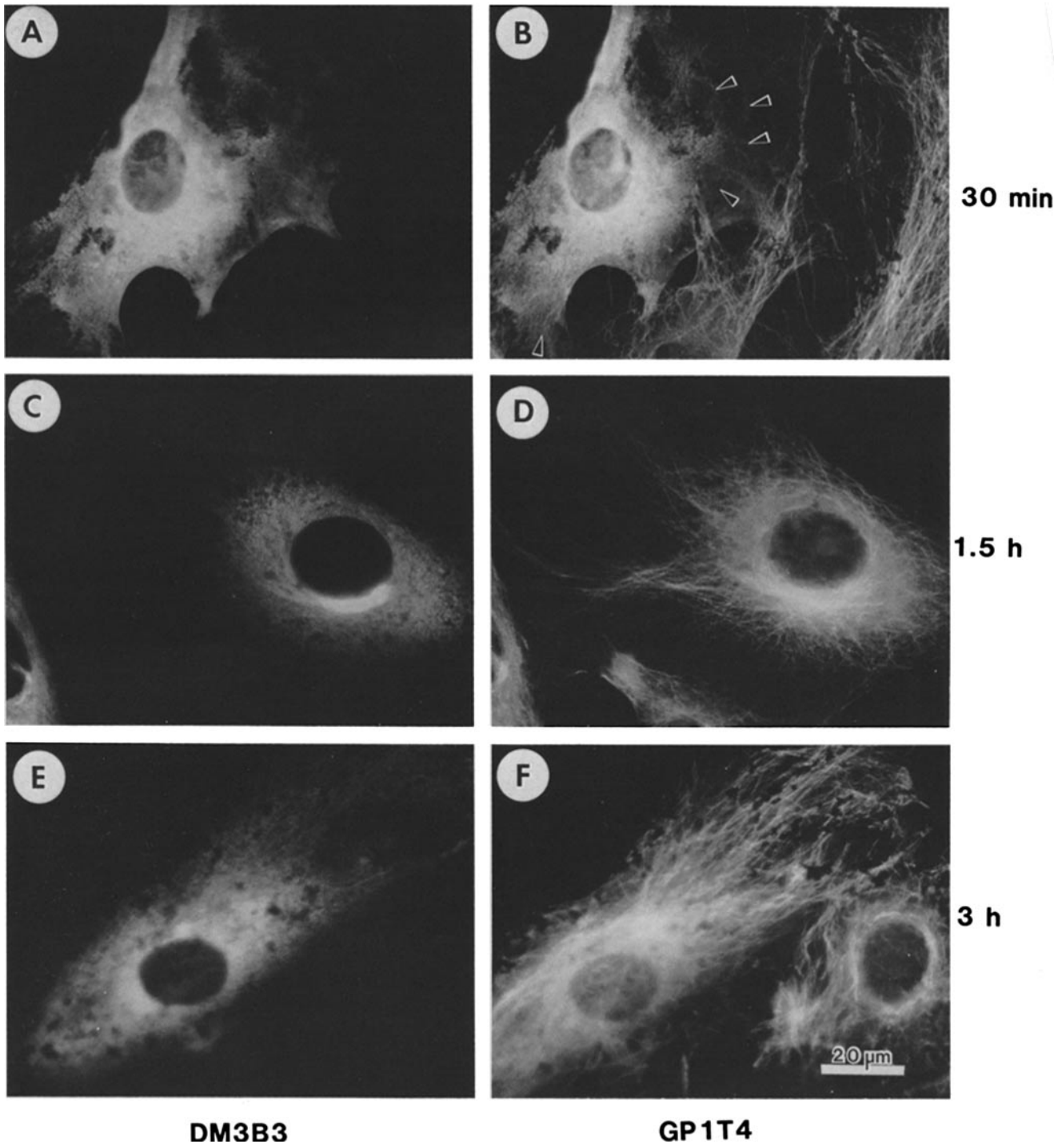

FIGURE 9 Fluorescence micrographs of cells microinjected with DM3B3 (monoclonal anti-β-tubulin) and stained to observe the microtubule distribution at 30 min (*A* and *B*), 1.5 h (*C* and *D*), and 3 h (*E* and *F*) after injection. Each pair, *A* and *B*, *C* and *D*, and *E* and *F*, represent the same cell stained for the distribution of DM3B3 with FITC-labeled goat anti-mouse (*A*, *C*, and *E*) and for the distribution of microtubules probed with TMRITC-labeled guinea pig antitubulin (GP1T4) (*B*, *D*, and *F*). At each time point the injected DM3B3 (*A*, *C*, and *E*) was found diffusely distributed in the cytoplasm. Within the first 30 min after injection the microtubules (*B*) were hard to visualize with GP1T4, except in the cell periphery (arrowheads). At 1.5 h postinjection (*D*) microtubules were observed in their normal radial array; and by 3 h postinjection the microtubules maintained their normal cytoplasmic distribution (*F*) at a time when the vimentin filaments were maximally collapsed. × 700.

peared to have no effect on the distributions of 10-nm filaments or microtubules (Fig. 7, *G–J*; Table I). In controls, cells injected with microinjection buffer or monoclonals against tropomyosin appeared to have no effect.

Several cells were injected in early prophase with DM3B3 and then fixed in metaphase. It appeared that the microtubules could assemble into a mitotic spindle that was surrounded by a 10-nm filament cage (Fig. 6, *G–J*).

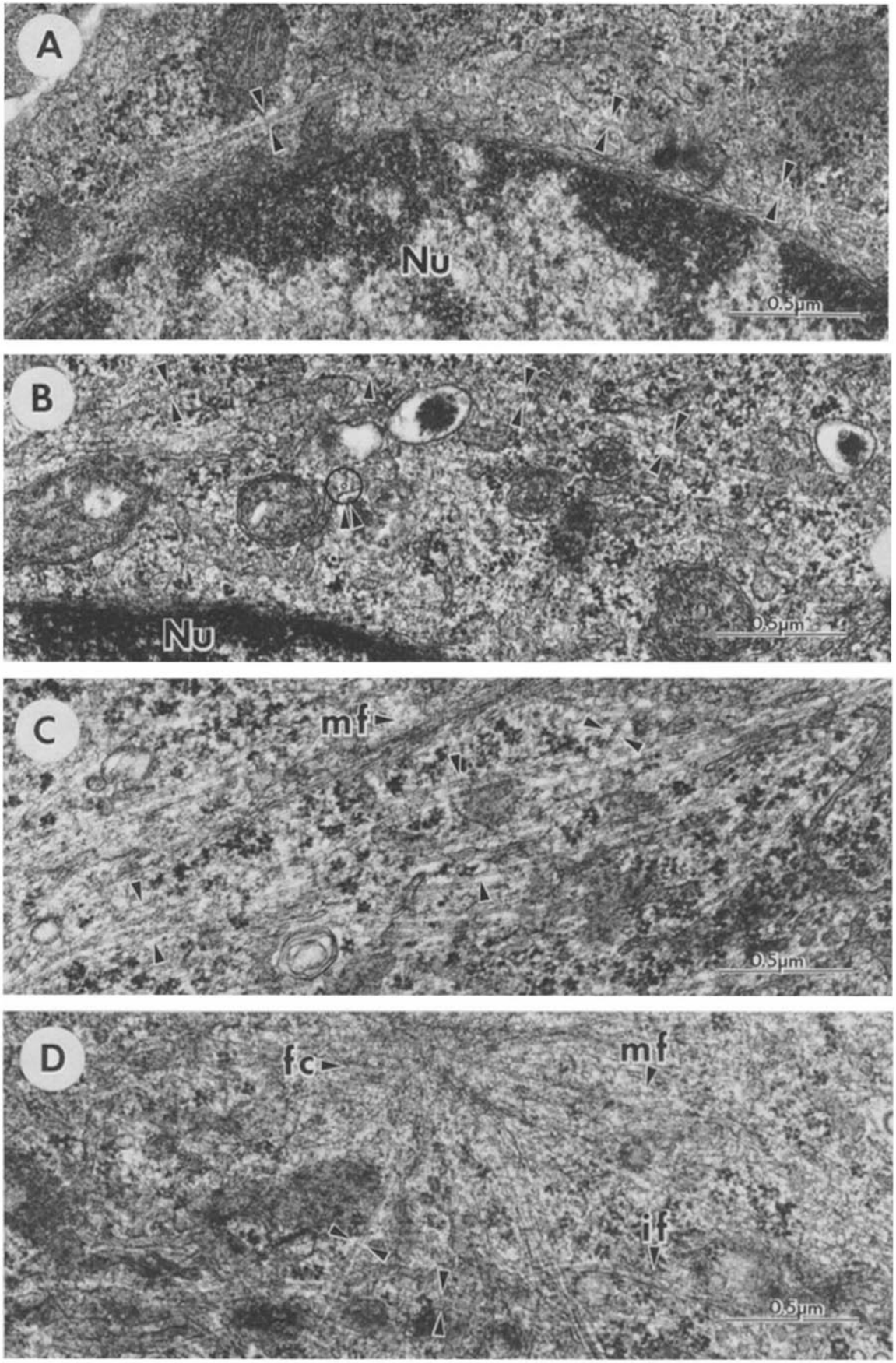

FIGURE 10 Electron micrographs of cells serially sectioned en face 30 min after microinjection with DM3B3. Abundant microtubule profiles were observed (between arrowheads) coursing through the cytoplasm for several micrometers near the nucleus (*A* and *B*). Occasionally cross-sectional profiles of microtubules could be observed (within the circle indicated by double arrowheads) near the nucleus (*B*). In the peripheral cytoplasm numerous microtubules (between arrowheads) were observed as well as microfilaments (*mf*) (C). Near the ventral surface of the cell (attachment side) microtubules (between arrowheads) were observed near focal contacts (*fc*) and 10-nm filaments (*if*) (*D*). *Nu*, nucleus. × 46,000.

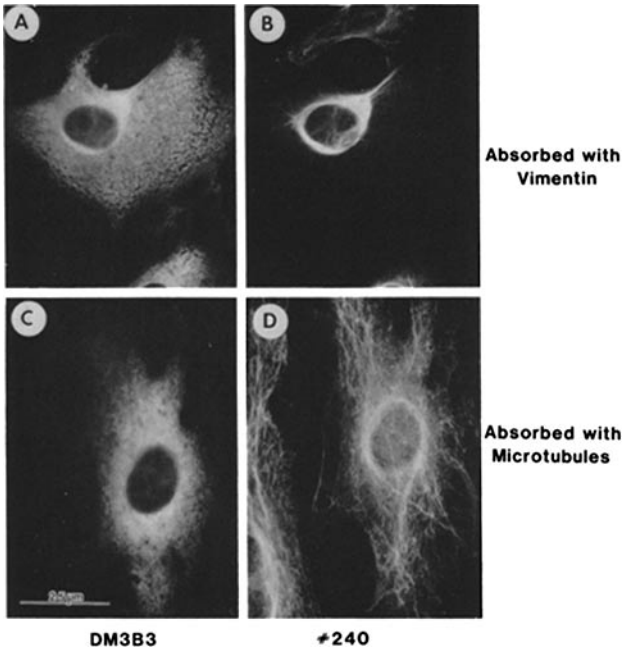

FIGURE 11 Fluorescence micrographs of cells microinjected with DM3B3 after it had been absorbed with CCL-146 vimentin (*A* and *B*) or absorbed with chick brain microtubules (C and D). Each pair, *A–B* and *C–D*, represents the same cell stained for the distribution of DM3B3 with FITC labeled goat anti-mouse (*A* and C) and for the distribution of the vimentin filaments with TMRITC-labeled antivimentin-#240 (*B* and *D*) 1.5 h after injection. When DM3B3 was absorbed with vimentin and then microinjected, the filaments capped (*A* and *B*). However, when DM3B3 was absorbed with microtubules and then injected, filament capping was abolished (*C* and *D*). × 480.

Microlabeling with [^{35}S]Methionine of Microinjected Cells

To determine the metabolic effects of microinjecting antitubulins on protein synthesis, we labeled microinjected cells with [^{35}S]methionine and then analysed by two-dimensional gel electrophoresis. Between 20–30 cells were microinjected on small (<1 mm^2) glass chips, then labeled in a small volume (10 μl), and analysed on two-dimensional gels as described in the Materials and Methods section. Cells that were analysed had been microinjected with the monoclonal or polyclonal antitubulins, microinjection buffer, or had not received any injection. In all cases, the microinjected cells continued to incorporate [^{35}S]methionine into their proteins in virtually an identical pattern to the control-uninjected cells (Fig. 12, *A* and *B*). The incorporation of [^{35}S]methionine into alpha- or beta-tubulin in injected or control cells appeared to be the same (Fig. 12, *C* and *D*). In some cases, the labeling of vimentin appeared to be slightly increased in experiments in which the microinjected antibody induced 10-nm filament disorganization (Fig. 12, *C* and *D*).

DISCUSSION

Recently several laboratories have reported generating monoclonal antibodies to tubulin (1, 29, 38, 63). We have generated five monoclonal antibodies and one polyclonal antibody to tubulin and microinjected these antibodies into cells. Only two of the monoclonals, one directed against alpha-tubulin (DM1A) and one against beta-tubulin (DM3B3), and the polyclonal antibody (GP1T4) caused the 10-nm filaments to collapse into aggregates within 1.5 h after microinjection. The majority of these lateral aggregates appeared to collapse more

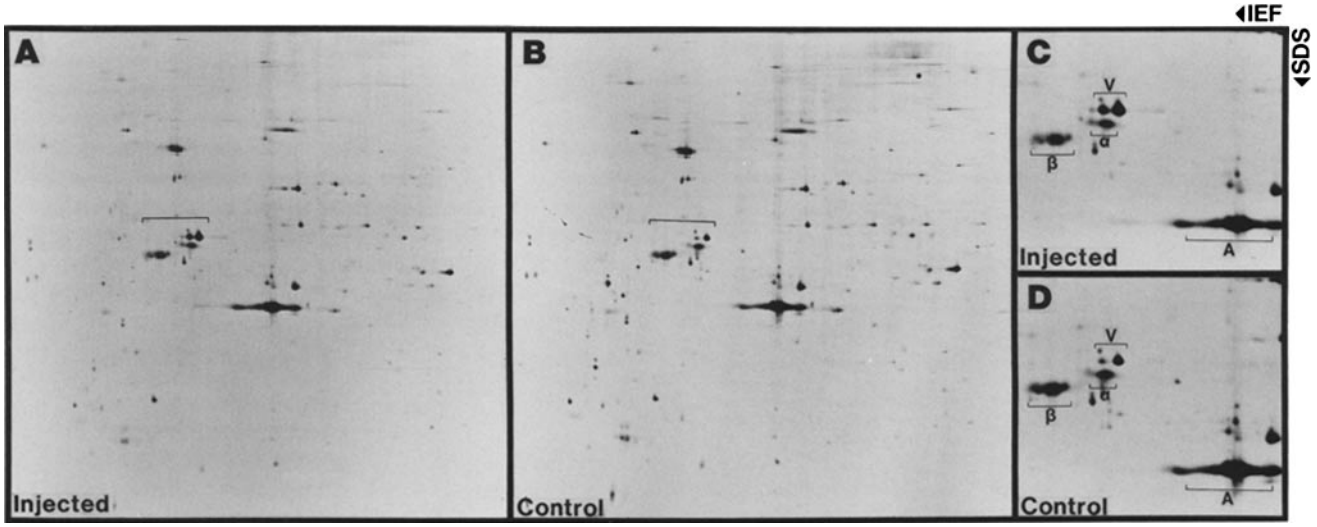

FIGURE 12 Fluorograms of two-dimensional gels analysing 25 injected cells (*A* and C) and 25 control-uninjected cells (*B* and *D*) microlabeled with [^{35}S]methionine according to the procedures detailed in the Materials and Methods. These experiments were done to determine the metabolic consequences of 10-nm filament disruption caused by microinjecting antitubulins (i.e, DM1A, DM3B3, GP1T4) into cells. (*A*) Fluorogram of the [^{35}S]methionine-labeled proteins of 25 cells microinjected with GP1T4; total counts applied were 121,965 cpm and the exposure was 1 month at −70°C. The area bracketed in *A* is enlarged in *C*. (*B*) Fluorogram of the [^{35}S]methionine-labeled proteins of 25 cells that were not injected; total counts applied were 119,775 cpm and the exposure was for 1 month at −70°C. The area bracketed in *B* is enlarged in *D*. In comparing the proteins of the injected cells versus the controls virtually an identical pattern was observed. When comparing the regions that contain actin (*A*), vimentin (*V*), alpha-tubulin (α), and beta-tubulin (β) in the injected (*C*) and control (*D*) cells there appears to be a slight increase in vimentin labelling in injected cells. This was occasionally observed in cells in which the microinjected antibody produced 10-nm filament disruption. Cells that were microinjected with buffer or other antibodies produced patterns indistinguishable from the controls. Isoelectric focusing was a 5–7 pH gradient and SDS 10% polyacrylamide gel electrophoresis was the second dimention. All fluorograms were developed, photographed, and printed under identical conditions.

slowly (1.5 h) and were not observed in studies in which the tight 10-nm filament caps were produced (10–15 min) in cells injected with antibodies directed against the vimentin cytoskeleton (23, 39, 46). The mechanism by which the antitubulin antibodies caused disorganization of the 10-nm filament system may have been initiated by a brief transient depolymerization of cytoplasmic microtubules within the first 30 min after antibody microinjection, since by immunofluorescence microscopy the central distribution of cytoplasmic microtubules was hard to evaluate. Electron microscopy of injected cells at this time detected assembled microtubules near the nucleus as well as the cell periphery although these observations were not quantitative. However, by the time filament disorganization had reached completion (1.5 h) the cytoplasmic array of microtubules appeared intact. By immunofluorescence these antibodies did not inhibit microtubules from assembling into a metaphase spindle in cells microinjected in early prophase and, in preliminary experiments, they did not block the temperature-dependent assembly of microtubules (S. H. Blose and F. Matsumura, manuscript in preparation). We abandoned the use of Taxol to stabilize cytoplasmic microtubules before microinjection because we found (unpublished observations) as others have (25), that Taxol treatment induces 10-nm filament disorganization. Therefore, it is possible that the injected antibodies may have exerted their effect by coating the microtubules. This could then disrupt the 10-nm filament–microtubule interactions, postulated by several structural (4, 8, 17, 24, 26, 32, 53, 55, 58) and biochemical studies (43, 54, 55). Because only certain antibodies to tubulin produced an effect, it may be likely that these antibodies were directed against only certain sites on the microtubules seemingly involved in 10-nm filament interactions.

Many agents have been shown to alter the 10-nm filament distribution in cells, such as viral infection (2), heat shock (42, 61), butyrate ion (34), vanadate ion (64), cycloheximid (56), an uncoupler of oxidative phosphorylation, carbonylcyanide p-trifluoromethoxyphenylhydrazone (48), diphtheria toxin and exotoxin-A (56), androgen treatment (49), nerve growth factor (44), $AlCl_3$ (47), ultra-violet irridation (36), and muscle hypertrophy (3, 20, 21). These agents appear to alter cellular metabolism although the exact mechanism by which they change 10-nm filament distribution has yet to be elucidated. In the present study, we examined the metabolism of microinjected cells by microlabeling with [^{35}S]methionine. No apparent differences could be detected between microinjected and control cells in the labeling of their proteins on two-dimensional gels—with one exception. In several experiments the synthesis of vimentin appeared to be slightly increased. The basis for this is not known, but might reflect the perturbation of the vimentin–10-nm filaments. It is of interest to note that perturbations of the apparent subunit pool of tubulin by microinjection of tubulin into living cells specifically alters the rate of tubulin synthesis in these cells (16). It is possible that the rate of vimentin synthesis is modulated by an intact vimentin–10-nm filament array. In any case, these metabolic studies did demonstrate that microinjected cells continue normal protein synthesis as a sign of their vitality and that 10-nm filament collapse was not a sign of mortality. Because each monoclonal antibody reacts with a relatively small region of the tubulin molecule, it is possible that two (DM1A, DM3B3) react with important sites involved with 10-nm filament interaction and the other three presumably do not interact with such sites. This is illustrated in Fig. 7, *G–J*, where it is clear the monoclonal antibody binds to the microtubules after injection but has no apparent effect on 10-nm filament distribution. Although we do not understand how the monoclonal antibodies disrupt the 10-nm filament distribution (as shown in this study) due to their high specificity for tubulin and no other molecule, it seems very likely that these results offer direct evidence for the existence of 10-nm filament—microtubule interaction.

We are grateful for Dr. J. D. Watson's support and criticism of this work. Our thanks are extended to Phil Renna for excellent photofinishing work, Madeline Szadkowski for meticulous word processing of the manuscript, and Joe Suhan for electron microscopy preparations. We thank Dr. Jim Garrels of the Cold Spring Harbor gel computer facility for running the two-dimensional gels. Research funds were provided by National Heart, Lung, and Blood Institute grant HL23848, National Institutes of Health grant GM 28277, grants from the American Heart Association (Nassau Chapter) and Muscular Dystrophy Association of America, Inc., and National Cancer Institute Cancer Center grant CA13106 to Cold Spring Harbor Laboratory.

Received for publication 20 July 1983, and in revised form 1 November 1983.

Note Added in Proof: After this manuscript was accepted Wehland and Willingham (Wehland, J., and M. C. Willingham, 1983, *J. Cell Biol.*, 97:1476–1490) reported that microinjection into cells of a concentrated monoclonal antibody against tyrosylated alpha-tubulin caused the 10-nm filaments to from perinuclear bundles and the microtubules to form perinuclear aggregates.

REFERENCES

1. Asai, D. J., C. J. Brokaw, W. C. Thompson, and L. Wilson. 1982. Two different monoclonal antibodies to alpha-tubulin inhibit the bending of reactivated sea urchin spermatozoa. *Cell Motility.* 2:599–614.
2. Ball, E. H., and S. J. Singer. 1981. Association of microtubules and intermediate filaments in normal fibroblasts and its disruption upon transformation by a temperature-sensitive mutant of Rous sarcoma virus. *Proc. Natl. Acad. Sci. USA.* 78:6986–6990.
3. Berner, P. F., A. V. Somlyo, and A. P. Somlyo. 1981. Hypertrophy-induced increase of intermediate filaments in vascular smooth muscle. *J. Cell Biol.* 88:96–101.
4. Bertolini, B., G. Monaco, and A. Rossi. 1970. Ultrastructure of a regular arrangement of microtubules and neurofilaments. *J. Ultrastruct. Res.* 33:173–186.
5. Blattler, D. P., F. Garner, K. Van Slyke, and A. Bradley. 1972. Quantitative electrophoresis in polyacrylamide gels of 2–40%. *J. Chromatogr.* 64:147–155.
6. Blose, S. H. 1979. Ten-nanometer filaments and mitosis: maintenance of structural continuity in dividing endothelial cells. *Proc. Natl. Acad. Sci. USA.* 76:3372–3376.
7. Blose, S. H. 1981. The distribution of 10 nm filaments and microtubules in endothelial cells during mitosis: double-label immunofluorescence study. *Cell Motility.* 1:417–431.
8. Blose, S. H., and A. Bushnell. 1982. Observations on the vimentin-10-nm filaments during mitosis in BHK-21 cells. *Exp. Cell Res.* 142:57–62.
9. Blsoe, S. H., and S. Chacko. 1976. Ring of intermediate (100 Å) filament bundles in the perinuclear region of vascular endothelial cells: their mobilization by colcemid and mitosis. *J. Cell Biol.* 70:459–466.
10. Blose, S. H., F. Matsumura, and J. J.-C. Lin. 1982. Structure of vimentin 10-nm filaments probed with a monoclonal antibody that recognizes a common antigenic determinant on vimentin and tropomyosin. *Cold Spring Harbor Symp. Quant. Biol.* 46:455–463.
11. Blose, S. H., and D. I. Meltzer. 1981. Visualization of the 10-nm filament-vimentin rings in vascular endothelial cells *in situ*: close resemblance to vimentin cytoskeletons found in monolayers *in vitro*. *Exp. Cell Res.* 135:299–309.
12. Blose, S. H., M. L. Shelanski, and S. Chacko. 1977. Localization of bovine brain filament antibody on intermediate (100 Å) filaments in guinea pig vascular endothelial cells and chick cardiac muscle cells. *Proc. Natl. Acad. Sci. USA.* 74:662–665.
13. Bonner, W. M., and R. A. Laskey. 1974. A film detection method for tritium-labeled proteins and nucleic acids in polyacrylamide gels. *Eur. J. Biochem.* 46:83–88.
14. Burnett, W. N. 1981. "Western blotting": electrophoretic transfer of proteins from sodium dodecyl sulfate-polyacrylamide gels to unmodified nitrocellulose and radiographic detection with antibody and radioiodinated protein A. *Anal. Biochem.* 112:195–203.
15. Cleveland, D. W., S. G. Fischer, M. W. Kirschner, and U. K. Laemmli. 1977. Peptide mapping by limited proteolysis in sodium dodecyl sulfate and analysis by gel electrophoresis. *J. Biol. Chem.* 252:1102–1106.
16. Cleveland, D. W., M. F. Pittenger, and J. R. Feramisco. 1983. Elevation of tubulin levels by microinjection suppresses new tubulin synthesis. *Nature (Lond.).* 305:738–740.
17. Ellisman, M. H., and K. R. Porter. 1980. Microtrabecular structure of the axoplasmic matrix: visualization of cross-linking structures and their distribution. *J. Cell Biol.*

876:464–479.
18. Feramisco, J. R. 1979. Microinjection of fluorescently labeled alpha-actinin into living fibroblasts. *Proc. Natl. Acad. Sci. USA.* 76:3967–3971.
19. Feramisco, J. R., and S. H. Blose. 1980. Distribution of fluorescently labeled alpha-actinin in living and fixed fibroblasts. *J. Cell Biol.* 86:608–615.
20. Ferrans, V. J., and W. C. Roberts. 1973. Intermyofibrillar connections in human and canine myocardium. An ultrastructural study. *J. Mol. Cell. Cardiol.* 5:247–257.
21. Gabella, G. 1979. Hypertrophic smooth muscle. IV. Myofilaments, intermediate filaments, and some mechanical properties. *Cell Tissue Res.* 201:277–288.
22. Garrels, J. I. 1979. Two-dimensional gel electrophoresis and computer analysis of proteins synthesized by clonal cell lines. *J. Biol. Chem.* 254:7961–7977.
23. Gawlitta, W., M. Osborn, and K. Weber. 1981. Coiling of intermediate filaments induced by microinjection of a vimentin-specific antibody does not interfere with locomotion and mitosis. *Eur. J. Cell Biol.* 26:83–90.
24. Geiger, B., and S. J. Singer. 1980. Association of microtubules and intermediate filaments in chicken gizzard cells as detected by double immunofluorescence. *Proc. Natl. Acad. Sci. USA.* 77:4769–4773.
25. Geuens, G., M. de Brabander, R. Nuydens, and J. De Mey. 1983. The interaction between microtubules and intermediate filaments in cultured cells treated with taxol and nocodazole. *Cell Biol. Int. Rep.* 7:35–47.
26. Goldman, R. D., and D. M. Knipe. 1972. Functions of cytoplasmic fibers in non-muscle cell motility. *Cold Spring Harbor Symp. Quant. Biol.* 37:523–534.
27. Goldman, R. D., A. Milsted, J. A. Schloss, J. Starger, and M. J. Yerna. 1979. Cytoplasmic fibers in mammalian cells: cytoskeletal and contractile elements. *Annu. Rev. Physiol.* 41:703–722.
28. Gordon, W. E., A. Bushnell, and K. Burridge. 1978. Characterization of the intermediate (10 nm) filaments of cultured cells using an autoimmune rabbit antiserum. *Cell.* 13:249–261.
29. Gozes, I., and C. J. Barnstable. 1982. Monoclonal antibodies that recognize discrete forms of tubulin. *Proc. Natl. Acad. Sci. USA.* 79:2579–2583.
30. Graessmann, A., M. Graessmann, and C. Mueller. 1980. Microinjection of early SV40 DNA fragments and T-antigen. *Methods Enzymol.* 65:816–825.
31. Hiller, G., and K. Weber. 1978. Radioimmunoassay for tubulin: a quantitative comparison of the tubulin content of different established tissue culture cells and tissues. *Cell.* 14:795–804.
32. Hirokawa, N. 1982. Cross-linker system between neurofilaments, microtubules, and membranous organelles in frog axons revealed by the quick-freeze, deep-etching method. *J. Cell Biol.* 94:129–142.
33. Holtzer, H., J. Croop, S. Dienstman, H. Ishikawa, and A. P. Somlyo. 1975. Effects of cytochalasin B and colcemid on myogenic cultures. *Proc. Natl. Acad. Sci. USA.* 72:513–517.
34. Hormia, M., E. Linder, V. P. Lehto, T. Vartio, R. A. Badley, and I. Virtanen. 1982. Vimentin filaments in cultured endothelial cells form butyrate-sensitive juxtanuclear masses after repeated subculture. *Exp. Cell Res.* 138:159–166.
35. Hynes, R. O., and A. T. Destree. 1978. 10 nm filaments in normal and transformed cells. *Cell.* 13:151–163.
36. Jimbow, K., and T. B. Fitzpatrick. 1975. Changes in distribution patterns of cytoplasmic filaments in human melanocytes during ultraviolet-mediated melanin pigmentation. The role of the 100 Å filaments in the elongation of melanocytic dendrites and in the movement and transfer of melanosomes. *J. Cell Biol.* 65:481–488.
37. Kennett, R. H. 1980. Fusion protocols: fusion by centrifugation of cells suspended in polyethylene glycol. *In* Monoclonal Antibodies: Hybridomas: A New Dimension in Biological Analyses. R. H. Kennett and T. J. McKearn, editors. Plenum Press, New York. 365–367.
38. Kilmartin, J. V., B. Wright, and C. Milstein. 1982. Rat monoclonal antitubulin antibodies derived by using a new non-secreting rat cell line. *J. Cell Biol.* 93:576–582.
39. Klymkowsky, M. 1981. Intermediate filaments in 3T3 cells collapse after intracellular injection of a monoclonal anti-intermediate filament antibody. *Nature (Lond.).* 291:249–251.
40. Laemmli, U. K. 1970. Cleavage of structural proteins during the assembly of the head of bacteriophage T4. *Nature (Lond.).* 227:680–685.
41. Lazarides, E. 1976. Two general classes of cytoplasmic actin filaments in tissue culture cells: the role of tropomyosin. *J. Supramol. Struct.* 5:531–563.
42. Leak, L. V., and F. Kato. 1972. Electron microscopic studies of lymphatic capillaries during early inflammation. I. Mild and severe thermal injuries. *Lab. Invest.* 25:572–588.
43. Leterrier, J. F., R. K. H. Liem, and M. L. Shelanski. 1982. Interactions between neurofilaments and microtubule-associated proteins: a possible mechanism for intraorganellar bridging. *J. Cell Biol.* 95:982–986.
44. Levi-Montalcini, R., and P. U. Angeletti. 1968. Biological aspects of nerve growth factor. *In* Growth of the Nervous System. G. E. W. Wolstenholme, and M. O'Connor, editors. Ciba Foundation Symposium. Little, Brown, and Co., Boston, 126–147.
45. Lin, J. J.-C., K. Burridge, S. H. Blose, A. Bushnell, S. A. Queally, and J. R. Feramisco. 1982. Use of monoclonal antibodies to study the cytoskeleton. *In* Cell and Muscle Motility. R. M. Dowben and J. W. Shay, editors. Plenum Publishing, New York. 2:63–71.
46. Lin, J. J.-C., and J. R. Feramisco. 1981. Distruption of the *in vivo* distribution of the intermediate filaments in fibroblasts through the microinjection of a specific monoclonal antibody. *Cell.* 24:185–193.
47. Liwnicz, B. H., K. Kristensson, H. M. Wisniewski, M. L. Shelanski, and R. D. Terry. 1974. Observations on axoplasmic transport in rabbits with aluminum-induced neurofibrillary tangles. *Brain Res.* 80:413–420.
48. Maro, B., and M. Bornens. 1982. Reorganization of HeLa cell cytoskeleton induced by an uncoupler of oxidative phosphorylation. *Nature (Lond.).* 295:334–336.
49. Nickerson, P. A., R. F. Skelton, and A. Molteni. 1970. Observation of filaments in the adrenal of androgen-treated rats. *J. Cell Biol.* 47:227–280.
50. Olmsted, J. B. 1981. Tubulin pools in differentiating neuroblastoma cells. *J. Cell Biol.* 89:418–423.
51. Osborn, M., and K. Weber. 1976. Cytoplasmic microtubules in tissue culture cells appear to grow from an organizing structure towards the plasma membrane. *Proc. Natl. Acad. Sci. USA.* 73:867–871.
52. Osborn, M., and K. Weber. 1977. The display of microtubules in transformed cells. *Cell.* 12:561–571.
53. Ramaekers, F. C. S., M. Osborn, E. Schmid, K. Weber, H. Bloemendal, and W. W. Franke. 1980. Identification of the cytoskeletal proteins in lens-forming cells, a special epithelioid cell type. *Exp. Cell Res.* 127:309–327.
54. Runge, M. S., and R. C. Williams. 1982. Formation of an ATP-dependent microtubule-neurofilament complex *in vitro*. *Cold Spring Harbor Symp. Quant. Biol.* 46:483–493.
55. Schliwa, M., and J. Van Blerkom. 1981. Structural interaction of cytoskeletal components. *J. Cell Biol.* 90:222–235.
56. Sharpe, A. H., L. B. Chen, J. R. Murphy, and B. N. Fields. 1980. Specific disruption of vimentin filament organization in monkey kidney CV-1 cells by diphtheria toxin, exotoxin A, and cycloheximid. *Proc. Natl. Acad. Sci. USA.* 77:7267–7271.
57. Sloboda, R. D., W. L. Dentler, R. A. Bloodgood, B. R. Telzer, S. Granett, and J. L. Rosenbaum. 1976. Microtubule-associated proteins (MAPs) and the assembly of microtubules *in vitro*. *Cold Spring Harbor Conf. Cell Proliferation.* 3(Book C):1171–1212.
58. Smith, D. S., U. Jarlfors, and B. F. Cameron. 1975. Morphological evidence for the participation of microtubules in axonal transport. *Ann. N.Y. Acad. Sci.* 253:472–506.
59. Spiegelman, B. M., S. M. Penningroth, and M. W. Kirschner. 1977. Turnover of tubulin and the N site GTP in chinese hamster ovary cells. *Cell.* 12:587–600.
60. Stacy, D. W., and V. G. Allfrey. 1976. Microinjection studies of duck globin messenger RNA translation in human and avian cells. *Cell.* 9:725–732.
61. Thomas, G. P., W. J. Welch, M. B. Mathews, and J. R Feramisco. 1982. Molecular and cellular effects of heat shock and related treatments of mammalian tissue culture cells. *Cold Spring Harbor Symp. Quant. Biol.* 46:985–996.
62. Titus, J. A., R. Haugland, S. O. Sharrow, and D. M. Segal. 1982. Texas red, a hydrophilic, red-emitting fluorophore for use with fluorescein in dual parameter flow microfluorometric and fluorescence microscopic studies. *J. Immunol. Methods.* 50:193–204.
63. Viklichy, V., P. Draber, J. Hasek, and J. Bartek. 1982. Production and characterization of a monoclonal antitubulin antibody. *Cell Biol. Int. Rep.* 6:725–731.
64. Wang, E., and P. W. Choppin. 1981. Effect of vanadate on intracellular distribution and function of 10 nm filaments. *Proc. Natl. Acad. Sci. USA.* 78:2363–2367.